International Journal of Mass Spectrometry 305 (2011) 50–57

Contents lists available at ScienceDirect

International Journal of Mass Spectrometry

journal homepage: www.elsevier.com/locate/ijms

Fast and metastable fragmentation of deprotonated D-fructose – A combined experimental and computational study

Helga D. Flosadottir, Ilko Bald*,[1], Oddur Ingólfsson*

University of Iceland, Department of Chemistry, Science Institute, Dunhagi 3, 107 Reykjavík, Iceland

ARTICLE INFO

Article history:
Received 4 May 2011
Received in revised form 26 May 2011
Accepted 26 May 2011
Available online 12 June 2011

Keywords:
Metastable decay
Monosaccharides
Matrix-assisted laser desorption and ionization
Classical dynamics simulations
Anions

ABSTRACT

Metastable and prompt fragmentation of the deprotonated monosaccharide D-fructose was studied. By using the isotope labelled molecules 1-^{13}C-D-fructose, 2-^{13}C-D-fructose and 6-^{13}C-D-fructose the origin of the observed fragments could unambiguously be identified. It was found that prompt fragmentation (<200 ns) is characterized by pronounced site selectivity, i.e. the neutral fragments contain C6 and the negative charge remains on the fragment containing the anomeric centre (C2). The selectivity is preserved in metastable dissociation (≈8 μs) only for the generation of the fragment ion $C_4H_4O_3^-$ (m/z 100). For all other metastable decay channels fragments with charge retention on the C6 containing fragment contribute appreciably. Density functional theory (DFT) and classical dynamics simulations are applied to predict the formation of fragment ions. Most of the experimentally detected fragment ions were also observed in the simulations thereby revealing detailed information about the fragmentation pathways. We found that the deprotonation site strongly influences the pathway of the dissociation reactions.

1. Introduction

Mono- and oligosaccharides are among the most common biomolecules, serving both as energy carrier and as structural component for all living organisms. Correspondingly, considerable effort has been dedicated to develop mass spectrometric and spectroscopic tools to characterize their structure and composition [1,2]. Furthermore, the subtle variances in saccharide structure and the resulting complexity of their mass spectra has motivated detailed studies of their fragmentation as potential means for structural characterisation and identification [3]. In this context, the fragmentation of different monosaccharides has been investigated by collision activation in tandem mass spectrometry, both in positive and negative ion mode [4,5].

The current interest in monosaccharide fragmentation is further motivated by the potential role of secondary low energy electrons in radiation damage to DNA [6,7] where the sugar moiety represents a pivotal building block. This has triggered studies on dissociative electron attachment (DEA) to both isolated ribose [8] and fructose [9] and the ribose monophoshate [10]. Recently, thin films of polysaccharide have been shown to change their properties markedly when exposed to low energy electrons [11]. This effect was attributed to DEA. Fragmentation studies on the isolated deprotonated sugars as well as ribose and deoxyribose in the respective nucleosides have also been conducted [12,13]. In these experiments the fragmentation of the anionic monosaccharides was found to be characterized by pronounced site selectivity, i.e. in the course of fragmentation the negative charge tends to remain on the anomeric carbon atom [8,12]. It was also shown that this selectivity is not determined by the mode of ionization (free electron attachment or deprotonation, respectively), but rather by the time scale of the dissociation reaction [12]. Direct DEA along a repulsive state proceeds generally very fast (in the order of vibrational periods, i.e. tens of fs) and the reaction pathway is governed by the involved electronic states of the anionic system [14]. In the case of low-energy electron attachment (<1 eV) to the pentose D-ribose this leads to dissociation by loss of C5 containing neutral fragments [8,15]. Interestingly, low-energy heavy-ion (≈10 eV) induced fragmentation of D-ribose also leads to a selective excision of C5 [16].

The characteristic fragmentation of deprotonated monosaccharides is a loss of different numbers of H_2O molecules and cross ring cleavage via abstraction of carbon containing fragments consisting of CH_2O units [4,12]. Due to the fairly simple composition of the monosaccharides, given by the CH_2O repeat-unit, conventional mass spectrometry on fragmentation of the native monosaccharides does not reveal much information on the underlying mechanism. In DEA this has been partly addressed by

* Corresponding authors.
E-mail addresses: ibald@zedat.fu-berlin.de (I. Bald), odduring@hi.is (O. Ingólfsson).
[1] Present address: Interdisciplinary Nanoscience Center (iNANO), Department of Physics and Astronomy, University of Aarhus, Denmark.

1387-3806/$ – see front matter © 2011 Elsevier B.V. All rights reserved.
doi:10.1016/j.ijms.2011.05.016

using isotopic labelled D-ribose and D-fructose as target molecules, however, the details of site selective fragmentation in deprotonated monosaccharides are much less explored. Recently we have used classical dynamics calculations to predict further fragmentation of the parent anion $[M–H]^-$ from the amino acid L-valine formed trough DEA and through deprotonation in the MALDI process [17]. For this fairly simple molecule the simulations reproduced the site selectivity of the dissociation processes well and showed clearly how different deprotonation sides lead to different fragmentation. More recently we have extended the application of our simulations to the nucleosides and deoxynucleosides constituting the DNA and RNA [13]. For these fairly large and complicated molecules the simulations reproduced the bond selectivity seen in the experiments very well. Furthermore, by selectively blocking the different deprotonation sites at the base and the sugar units, we could determine unambiguously what deprotonation sites lead to the individual fragmentation channels. These results were also well reproduced in our simulations.

Here we report on a study aimed at understanding details about the mechanism behind specific fragmentation reactions of the monosaccharide D-fructose and the conditions under which selective bond breaking occurs. For this purpose we have studied fast and metastable decay of the deprotonated isotopic labelled 1-^{13}C-, 2-^{13}C- and 6-^{13}C-D-fructose. To further verify the mechanism behind the individual fragmentation processes and to understand the role of individual deprotonation sites we compliment our experimental results with classical dynamics simulations.

2. Methods

2.1. MALDI-experiments

Fast (prompt) and metastable decay of isotope labelled D-fructose (1-^{13}C-D-fructose, 2-^{13}C-D-fructose, 6-^{13}C-D-fructose) was measured in in-source decay (ISD) and post-source decay (PSD) mode, respectively, on a commercial matrix assisted laser desorption and ionization (MALDI) instrument (Reflex IV, Bruker Daltonics). The instrument is equipped with a reflectron time-of-flight mass spectrometer (ToF-MS) and an N_2 desorption laser (337 nm, repetition rate 10 Hz). The ions are extracted with a delay time of 200 ns and accelerated into the field-free flight tube with a double focusing Wiley McLaren acceleration optics. The operation of the instrument to measure fast (ISD) and metastable (PSD) decay has been described in detail elsewhere [18]. Briefly, the ISD spectra were all recorded in reflectron mode and the laser power was set to be about 10% above the detection threshold for the deprotonated molecule. The PSD spectra were recorded by gating the deprotonated molecules into the field free linear flight tube. The desorption laser power was kept about 20% above the detection threshold for the corresponding ion. The laser spot was moved manually over the sample during acquisition to average out sample inhomogeneity. The acceleration voltage into the linear region was 25 kV resulting in about 8 μs flight time, which is the time window within which we observe metastable decay. The width of the mass gate was ±5 Da in all experiments. After the linear flight the ions are decelerated and reaccelerated with a grid-less reflectron and detected on a double micro-channel plate detector. The reflectron voltage is stepped down in 7 segments to assure for collection of all fragments. Individual segments are the sum of 500 shots, which were recorded by using the fragmentation analyses and structural ToF method FAST, within the instrumental control software FlexControl®. The alignment of individual segments and the mass calibration of the spectra was carried out with the FlexAnalyses® software also provided by the instrument manufacturer.

D-Fructose was purchased from Sigma–Aldrich (St. Louis, MO, USA) with a stated purity ≥99% and the isotope labelled analogues 1-^{13}C-D-fructose, 2-^{13}C-D-fructose and 6-^{13}C-D-fructose were obtained from Cambridge Isotope Laboratories, Inc. (Andover, MA, USA) with a stated purity of 99%. All compounds were used without further purification.

Samples were prepared by pre-spotting 0.5 μL of a 2.8 mM aqueous solution of bisbenzimide hydrochloride matrix; $C_{25}H_{24}N_6O{\cdot}3HCl$, from Sigma–Aldrich (St. Louis, MO, USA) on a stainless steel sample carrier. After drying the matrix in air, 0.5 μL of a 0.13 M solution of D-fructose in methanol was spotted on the matrix and allowed to dry.

2.2. Classical dynamics simulations

To identify possible fragmentation channels we have conducted classical dynamics simulations of various dissociation processes for both α and β D-fructopyranose. The calculations have been described in detail elsewhere [13]. We thus only give a brief description here. We used density functional theory (DFT) with a plane wave basis set (energy cut-off at 395.994 eV) and the PW91 functional as implemented in the VASP code [19,20]. Geometric energy minimization using damped molecular dynamics and conjugate gradient algorithm to relax the system to its ground state was carried out for neutral α- and β-D-fructose, and the five different deprotonated molecules of α- and β-D-fructose, respectively. The neutral D-fructose system was then heated to room temperature by scaling the velocities of the atoms to give an internal energy corresponding to 298 K. The vibrational modes were allowed to equilibrate in a dynamics simulation for 1000 fs. The simulation was then continued for another 1000 fs from which 10 configurations, separated by a time interval of 100 fs, were taken and used as starting points for further simulations of the fragmentation process. For each investigated parent ion (deprotonation site) the respective proton was removed from all 10 geometries. An internal energy of 8 eV was then added to account for the internal energy acquired in the MALDI process. Finally constant energy (microcanonical) simulations of 500 fs were carried out for the highly vibrationally excited, deprotonated molecules. The resulting statistical fragmentation pathways were documented and the charge of each fragment was determined by the Bader's method [21–23].

During the desorption and ionization process in MALDI small molecules acquire approximately 4–5 eV internal energy [24], and the experimental time window of metastable fragmentation in our measurements was about 8 μs. Due to limited computational time and cost 500 fs was the chosen timeframe for the simulations. This is only a fraction of the experimental time window for the metastable decay. To induce fragmentation within the computational time window we have increased the internal energy inserted to the system to 8 eV, which increases the speed of fragmentation and other reactions such as rearrangement. It is important to be aware that increasing the internal energy may also open new fragmentation channels, which are not available for a system with 4–5 eV internal energy. On the other hand we cannot avouch for the simulations to cover the whole potential energy surface, and since the fragmentation channels were accelerated by high internal energy, the more probable or faster fragmentation channel is generated during the dynamic simulation while the less efficient may not be observed at all. In total we performed 50 simulations (10 for each deprotonation site), and for each deprotonation site we observed 4–7 different fragmentation pathways that are summarized in Table S1 of the Supplementary material.

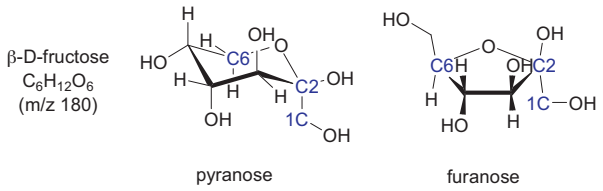

Fig. 1. Molecular structure of β-D-fructopyranose and β-D-fructofuranose. Positions 1, 2 and 6 are highlighted corresponding to the positions of isotope labelling used in the present study.

3. Results and Discussion

3.1. Structure and acidity of D-fructose

D-Fructose can adopt four isomeric structures, the α- or β-pyranose structure, and the α- or β-furanose structure (Fig. 1). When bound within oligo- and disaccharides D-fructose usually adopts the furanose form, whereas in aqueous solution of the monomer equilibrium between pyranose and furanose evolves with the pyranose being dominant. D-Fructose crystallises as β-pyranose [25], and quantum mechanical and molecular mechanics calculations of the structure of D-fructose indicate that in the solid phase indeed the β-pyranose tautomer is the most stable among all possible isomers [26]. The gas phase structure, however, is more difficult to predict [26]. A recent experimental and theoretical study on the gas phase structure of monosaccharides indicated that during laser desorption the crystal structure of monosaccharides is preserved [27]. Hence, for the present work it is reasonable to assume that D-fructose is present as the six-membered ring, i.e. the pyranose form, and as the β-anomer. Nevertheless, it is possible that the present sample also contains a certain amount of α-pyranose tautomer.

During the MALDI process D-fructose is deprotonated, and the proton can basically be removed from any of the five hydroxyl groups. So far the individual acidities for the different deprotonation positions in D-fructose have not been reported. A computational study on D-glucose [28], however, showed that the hydroxyl group at the anomeric centre is the most acidic. Our classical dynamics simulations (see Section 3.3) indicate that in D-fructose the anomeric hydroxyl group (OH2) and OH5 are the most acidic.

3.2. Post-source and in-source decay mass spectra

Fig. 2 compares the PSD spectra of the native D-fructose with the isotope marked analogues 1-^{13}C-D-fructose, 2-^{13}C-D-fructose and 6-^{13}C-D-fructose. Fig. 3 compares the ISD spectra for the same compounds. The sum formula for the observed fragment ions and a tentative assignment of the corresponding neutrals are summarized in Table 1 along with the matching fragments from the classical dynamics simulations.

The characteristic fragments from PSD of the native D-fructose are observed at *m/z* 161, 149, 143, 131, 119, 107, 100, 89 and 71.

The peaks appearing at *m/z* 161 and 143 correspond to the loss of one and two water molecules, respectively. Thus, there is no carbon loss associated with the formation of these fragments and correspondingly the peaks appear shifted up by one mass unit for all the ^{13}C labelled sugars.

The fragment at *m/z* = 149 in the spectrum of native D-fructose corresponds to the loss of one formaldehyde unit (CH_2O), consequently, it is the largest fragment formed through carbon loss. From Fig. 2 it can be seen that the mass of this fragment is partly shifted in the case of 1-^{13}C-D-fructose and 6-^{13}C-D-fructose, but appears exclusively at *m/z* = 150 for 2-^{13}C-D-fructose. Hence, the fragment is

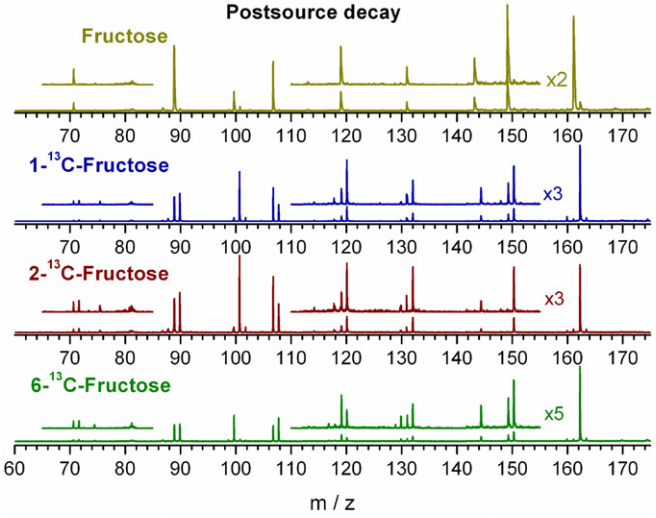

Fig. 2. Post-source decay spectra of D-fructose, 1-^{13}C-D-fructose, 2-^{13}C-D-fructose and 6-^{13}C-D-fructose.

formed by a terminal loss of a CH_2O unit from either the C1 or the C6 end. In both 1-^{13}C-D-fructose and 6-^{13}C-D-fructose the ratio of the *m/z* 149 and *m/z* 150 signal are found to be comparable, indicating that the C1 and the C6 loss are comparably likely.

The fragment from native D-fructose that appears at *m/z* 131 is assigned to the loss of H_2O and a CH_2O unit. The intensity ratios of the corresponding signals at *m/z* 131 and 132 in the PSD spectra of 1-^{13}C-D-fructose and 2-^{13}C-D-fructose are very similar and in both cases the signal at *m/z* 132 dominates. In the PSD spectra of 6-^{13}C-D-fructose fragment peaks appear at *m/z* 132, 131 and 130. Also here, the signal at *m/z* 132 dominates. If we only consider terminal carbon loss, the *m/z* 132 peak from 1-^{13}C-D-fructose and 2-^{13}C-D-fructose must be due to C6 loss. From 6-^{13}C-D-fructose, on the other hand, the *m/z* 132 signal must be due to C1 loss. It is thus clear that both C1 and C6 loss contribute to the signal observed at *m/z* 131 for the native D-fructose. It is, however, not conclusive from the PSD spectra to what extent the C1 and C6 loss contribute to this fragment or if there is possibly some contribution from non-terminal carbon loss.

The fragment that appears at *m/z* 119 from native D-fructose shows complementary behaviour when we compare

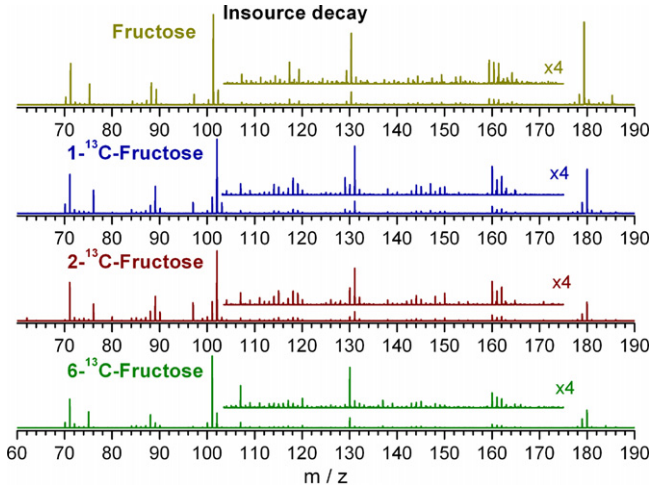

Fig. 3. In-source decay spectra of D-fructose, 1-^{13}C-D-fructose, 2-^{13}C-D-fructose and 6-^{13}C-D-fructose.

Table 1
Summary of anionic fragments observed in PSD, ISD and from classical dynamics of deprotonated D-fructose along with the neutral losses.

PSD fragment anions			ISD fragment anions			Simulations		
m/z	Fragment	Neutral loss	*m/z*	Fragment	Neutral loss	*m/z*	Fragment	Neutral loss
161	$C_6H_9O_5^-$	H_2O	160	$C_6H_8O_5^-$	H_2O+H	161	$C_6H_9O_5^-$	H_2O
149	$C_5H_9O_5^-$	CH_2O				149	$C_5H_9O_5^-$	CH_2O
143	$C_6H_7O_4^-$	$2H_2O$						
131	$C_5H_7O_4^-$	CH_2O+H_2O	130	$C_5H_6O_4^-$	CH_2O+H_2O+H	131	$C_5H_7O_4^-$	CH_2O+H_2O
119	$C_4H_7O_4^-$	$C_2H_4O_2$				119	$C_4H_7O_4^-$	$C_2H_4O_2$
107	$C_3H_7O_4^-$	$C_3H_4O_2$						
100	$C_4H_4O_3^-$	$C_2H_4O_2+H_2O+H$	101	$C_4H_4O_3^-$	$C_2H_4O_2+H_2O$	101	$C_4H_4O_3^-$	$C_2H_4O_2+H_2O$
89	$C_3H_5O_3^-$	$C_3H_6O_3$	89	$C_3H_5O_3^-$	$C_3H_6O_3$	89	$C_3H_5O_3^-$	$C_3H_6O_3$
			88	$C_3H_4O_3^-$	$C_3H_7O_3$			
			75	$C_3H_7O_2^-$	$C_3H_4O_4$			
			71	$C_3H_3O_2^-$	$C_3H_6O_3+H_2O$			

6-^{13}C-D-fructose with 1-^{13}C-D-fructose and 2-^{13}C-D-fructose. In 6-^{13}C-D-fructose the intensity ratio between *m/z* 119 and 120 is about 2:1 in favour of *m/z* 119. Hence, about 2/3 of the signal is due to the loss of the 6-^{13}C. From 1-^{13}C-D-fructose and 2-^{13}C-D-fructose, on the other hand, only about 1/3 of the signal is due to the loss of the respective ^{13}C's. This complementary behaviour and the fact that the intensity ratios for this fragment are identical for 1-^{13}C-D-fructose and 2-^{13}C-D-fructose is consistent with terminal loss of a $C_2H_4O_2$ unit rather than the loss of two CH_2O units. The branching ratios between both fragmentation channels are 2:1 in favour of the neutral (C6)H_2O–(C5)H_2O loss.

The fragmentation channel at *m/z* 107 also shows complementary behaviour when we compare 6-^{13}C-D-fructose with 1-^{13}C-D-fructose and 2-^{13}C-D-fructose. Now the branching ratio is about 2:1 in favour of the loss of C1 and C2. This fragment was earlier tentatively assigned to a cross ring cleavage exclusively leading to a charged fragment containing C1, C2 and C3 [12]. From the current data, however, it is apparent that, though to a lesser extent, also a negatively charged fragment containing C6 is formed.

The most remarkable selectivity in the PSD spectra is observed for *m/z* 100. Here we observe as good as no shift from 6-^{13}C-D-fructose, but close to 100% of the ion signal from 1-^{13}C-D-fructose and 2-^{13}C-D-fructose is shifted by one Dalton. This channel can thus only be explained by a close to 100% selective loss of H_2O and a $C_2H_5O_2$ unit containing both C1 and C2.

Finally, two more channels are observed in the PSD spectra; one at *m/z* 89 and one at *m/z* 71. Both these channels constitute the loss of three carbon atoms and no particular selectivity is observed. The slight difference in intensity observed at *m/z* 89 and 90 for the isotope labelled sugars is always present and is assigned to the natural abundance of ^{13}C.

The ISD spectra of native D-fructose (Fig. 3) are characterized by signals around *m/z* 160, 130, 101, 89, 88, 75 and 71. The contributions around *m/z* 160 are attributed to the loss of one H_2O unit from the deprotonated molecule (at *m/z* 161) and the additional loss of one and two hydrogen (at *m/z* 160 and 159, respectively). Correspondingly, the ^{13}C labelled D-fructoses show the same pattern and are shifted by one mass unit with respect to the native D-fructose. The fragments at *m/z* 130, 101, 89, 88, 75 and 71 on the other hand all correspond to the loss of one or more carbon atoms. The signal at *m/z* 130 matches the loss of one CH_2O unit, one H_2O and one hydrogen atom from the deprotonated molecule and *m/z* 101 corresponds to the loss of a $C_2H_4O_2$ unit and an H_2O from the deprotonated molecule. The fragment ions at *m/z* 89/88 and 75 correspondingly represent the loss of at least three carbon atoms. In the first case the mass difference to the neutral precursor corresponds to the loss of a $C_3H_6O_3$ unit (*m/z* 89) or a $C_3H_7O_3$ unit (*m/z* 88). In the latter case (*m/z* 75) the resulting negative fragment ion is concordant with the sum formula $C_3H_7O_2^-$. Finally, *m/z* 71 matches the sum formula $C_3H_3O_2^-$.

Most remarkable about the ISD spectra displayed in Fig. 3 is the fact that with the exception of *m/z* 89/88 and 71, all the fragmentation processes associated with carbon loss, nearly exclusively result from a terminal fragmentation from the C6 end. The mass ratios 89 and 88 still show preferable C6 loss though also C1 and C2 loss is observed to some extent. For *m/z* 71 there is no selectivity with regard to C6 *vs.* C1 loss. This fragment, however, appears nearly exclusively at *m/z* 71 in the ISD spectra of all three isotopic labelled compounds and nearly no signal is observed at *m/z* 72. Hence, the *m/z* 71 fragment is formed selectively through loss of C1, C2 and C6. In summary, the ISD is very selective and, with the exception of the *m/z* 71 fragment, nearly no ^{13}C1 or ^{13}C2 loss is observed. This even applies if the fragments result from the loss of as much as three carbon atoms, and is in clear contrast to the PSD spectra.

In general, the difference in selectivity of ISD and PSD fragmentation can be explained either in terms of different precursor ions or as an effect of the intrinsically distinct physical character of PSD and ISD. Different precursor ions can be different structural isomers (pyranose or furanose), diastereomers (α- and β-diastereomers), or isomers with different deprotonation sites. The main differences in the physical character of PSD and ISD are; (i) that in the ISD process individual molecules are likely to be considerably warmer before the multiple collisions in the expanding plume have lead to a thermal quasi-equilibrium [29], (ii) the fragmentation in ISD takes place under multiple collision conditions, and (iii) the time frame for ISD is much shorter than for PSD. In our experiments the pulsed ion extraction delay is set at 200 ns. Thus the ISD processes observed here are processes that are operative within the first 200 ns (and also partly during the extraction), the PSD processes on the other hand proceed within the linear flight time, which is about 8 μs. Furthermore, also the higher internal energy in ISD is evident when comparing the ISD and the PSD spectra. While there is appreciable contribution from a number of high mass fragments in the PSD spectra no fragments above *m/z* 100 contribute significantly to the ISD spectra. Hence, in the ISD we are observing the low mass tail of the decay series, i.e. stable fragments resulting from a number of preceding fragmentation steps. These factors are in favour of kinetically controlled fragmentation in ISD. Here we also observe selectivity in the fragmentation pathways in PSD, however, the selectivity is much higher in ISD. In PSD we observe preferable loss of one of the ^{13}C's on some of the channels but no preferences on others and only one fragment (*m/z* 100) is exclusively formed through carbon loss from only one side of the molecule (the C6 side). In ISD on the other hand nearly all fragments are close to be exclusively formed through 6-^{13}C loss and nearly no 1-^{13}C or 2-^{13}C loss is observed.

We explain the extraordinarily high selectivity in ISD by selective charge retention on the fragment carrying the anomeric centre (C2) rather than selective bond ruptures. The precursor ion carries the charge most likely at the anomeric centre that initiates

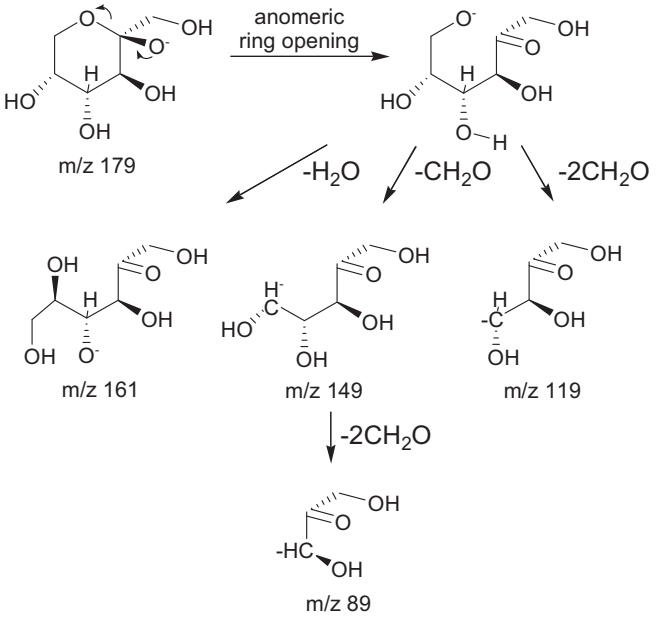

Fig. 4. Summary of dissociation products observed in classical dynamics simulations for β-D-fructose deprotonated at the anomeric hydroxyl group (OH2). The initial step in the fragmentation is a ring cleavage at the C2–O bond followed by loss of water and different neutral carbon-containing fragments from the C6 site of D-fructose.

the dissociation. Fast fragmentation (of hot molecular ions) in ISD therefore leads to selective charge retention on the anomeric centre. The metastable ions probed in PSD have lower internal energies than the precursor ions in ISD, and the internal energy is most likely redistributed over all available degrees of freedom (intramolecular vibrational redistribution, IVR). Thus, after several μs other fragmentation channels become accessible resulting in less selectivity.

In the next section we will discuss classical dynamics simulations that help to elucidate important details of the fragmentation reactions, especially the role of deprotonation sites for specific dissociation reactions.

3.3. Simulations of the fragmentation processes

In previous studies of metastable fragmentation of the amino acid L-valine [17] and the DNA/RNA nucleosides and deoxynucleosides [13] we have shown that classical dynamics simulations represent a powerful tool to predict dissociation pathways of deprotonated biomolecules. In the current study we have carried out classical dynamics simulations on the fragmentation of vibrationally activated α- and β-D-fructose in their ground electronic state when these are deprotonated at the various hydroxyl groups.

From deprotonated α- and β-D-fructose the main fragment ions in the classical dynamics simulations were found at *m*/*z* 161, 149, 119, 101, 89 and 59 agreeing very well with the fragmentation products observed in the experiments. The predicted fragmentation reactions leading to these fragment ions (except *m*/*z* 59) after deprotonation at the OH2 are summarized in Fig. 4.

In general, the precursor ions generated by initial deprotonation of a hydroxyl group in D-fructose are stabilized by intramolecular hydrogen bonds between the negatively charged oxygen and an adjacent hydroxyl group. The subsequent fragmentation reactions in our simulations were found to be composed of three characteristic reaction steps. These are (i) intramolecular proton transfer, (ii) anomeric ring opening, and (iii) antiperiplanar dissociation (see Supplementary material for more information). Basically all fragmentation reactions observed in our classical dynamics simulations can be described as a sequence of these reaction steps and the typical neutral elimination products are water, formaldehyde (CH_2O) and longer aldehydes.

The intramolecular proton transfer steps occur with low energy barriers and are thus frequently observed. The proton transfer proceeds also faster than dissociation via C–C bond breaking and consequently further dissociation preferably takes place when proton transfer has lead to charge location at the most acidic hydroxyl group. The number of observed intramolecular proton transfer reactions in a given number of simulations for a specific deprotonation site indicates that the acidity of the individual OH groups can be ordered in the following way: OH2 ≈ OH5 > OH1 > OH3 ≈ OH4. Almost no proton transfer is observed after deprotonation of OH2 or OH5. Instead various cross-ring cleavage reactions are induced from these anions. Anomeric ring opening is characteristic for deprotonation of OH2. This creates a ketone at C2, which in some cases leads to further fragmentation such as elimination of water (resulting in *m*/*z* 161) or loss of one or more CH_2O units as is depicted in Fig. 4. Deprotonation at OH1, on the other hand, results either in C1–C2 bond cleavage or proton transfer from OH2 and subsequent anomeric bond cleavage (see below). Deprotonation at OH3 or OH4 mainly results in proton transfer from the adjacent hydroxyl groups indicating that these hydroxyl groups have the lowest acidity. Antiperiplanar arrangement of the bonds to which the negatively charged oxygen and the leaving group are connected is a typical prerequisite for the dissociation channels observed. For instance, 70% of the dissociation reactions observed after deprotonation of OH5 proceed from an antiperiplanar conformation.

m/*z* 161. The fragment ion at *m*/*z* 161 represents the loss of one water molecule from the respective D-fructose and does not involve carbon loss. It is thus not possible to gain insight into this fragmentation channel through the mass spectra of the isotope marked ^{13}C-D-fructoses. Nevertheless, as this is the most pronounced signal in the PSD spectra it is worthwhile to have a closer look at this channel in our simulations. In the simulations this fragment is formed from the D-fructose when it is deprotonated at OH3, OH4 or OH5. Water loss is also observed after deprotonation at OH1 and OH2, but in both these cases this is either observed subsequent to a CH_2O loss or preceding the same (see below). Deprotonation at OH3, on the other hand, leads to proton transfer from OH2 in conjunction with an anomeric ring opening. Subsequently OH3 along with the hydrogen of OH4 is eliminated as H_2O and further fragmentation is not observed. Water loss after deprotonation at OH4 on the other hand, proceeds through an antiperiplanar dissociation rupturing the C3–C4 and the C2–OH bond. In this case OH2 with the hydrogen from OH1 is eliminated. This channel was only observed from the α-D-fructose, as such antiperiplanar dissociation is not possible from the β-anomer. Finally, from D-fructose deprotonated at OH5, we also find water elimination containing OH2 with the hydrogen from OH1. However, here the elimination is found to proceed under C1–O1–C2 epoxide formation without any direct involvement of the charge location site.

m/*z* 149. The predictive power of our simulation method can be demonstrated on the fragment with *m*/*z* 149, corresponding to the loss of a single CH_2O molecule from the deprotonated D-fructose. The mass spectra of isotope labelled D-fructose indicate that the carbon atom of CH_2O originates to a comparable extent from position 1 and 6 (see Section 3.2 and Fig. 2). Our classical dynamics simulations showed that the different origin is likely to be correlated with the initial position of deprotonation. Deprotonation at the anomeric centre (OH2) leads to a ring-opening, as it was previously observed for glucose [28], and subsequently to a formation of a C=O double bond, and abstraction of neutral CH_2O from the C6 site (Fig. 5a). Remarkably, deprotonation at position 1 results in six out of ten simulations in the formation of CH_2O from C1 as it is displayed in Fig. 5b. Hence, the classical dynamics simulations

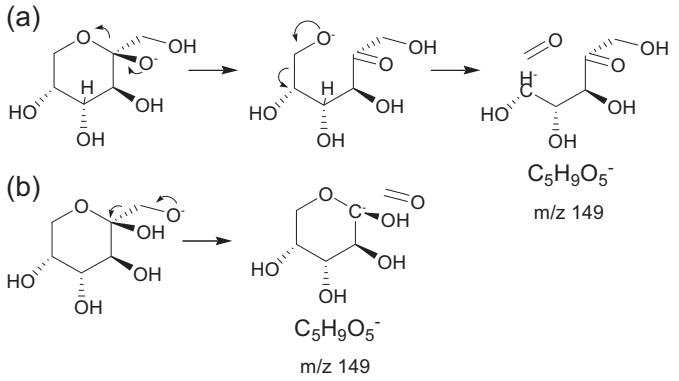

Fig. 5. Reaction scheme from the classical dynamics simulations showing how the loss of neutral CH_2O from the C1 site and the C6 site (leading to *m*/*z* 149) depends on the initial deprotonation site.

predicted a signal in the mass spectrum at *m*/*z* 149, the intensity of which is shifted by 50% to *m*/*z* 150 in both 1-^{13}C-D-fructose and 6-^{13}C-D-fructose, and completely shifted in 2-^{13}C-D-fructose. This is fully in agreement with the PSD mass spectra shown in Fig. 2.

m/*z* 131. The fragment ion at *m*/*z* 131 is assigned to the loss of a neutral water and a formaldehyde unit. Experimentally we have verified both C6 and C1 loss in this case, but from our mass spectra we cannot make conclusive statements about the relative contributions of these two channels. In our simulations both C1 and C6 loss was observed but deprotonation at OH1 exclusively results in elimination of C1. Here the β-anomer leads to C1 loss in six out of ten simulations (6/10), when deprotonated at OH1. In an additional step water is eliminated from OH5 and the hydrogen from OH2 (Fig. 6a). Also deprotonation at OH5 results in C1 loss subsequent to antiperiplanar water elimination (Fig. 6b). C6 loss is only observed from the α-anomer. An example is shown in Fig. 6c, in which deprotonation at OH2 induces anomeric bond cleavage and CH_2O elimination from C6 followed by water elimination from OH4 and the hydrogen of OH3.

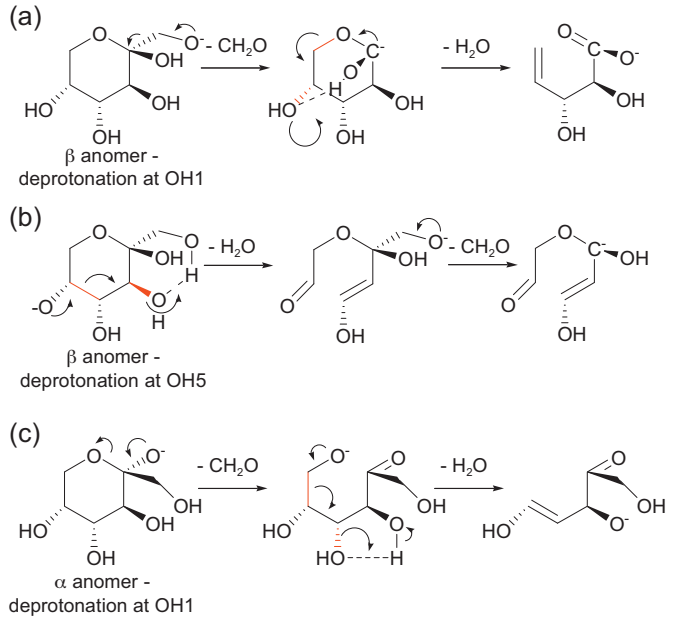

Fig. 6. Reaction scheme from the classical dynamics simulations showing the loss of neutral CH_2O and H_2O from the C6 site as well as from the C1 site (leading to *m*/*z* 131).

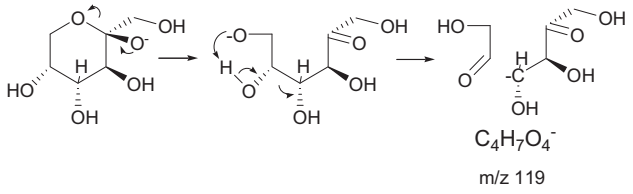

Fig. 7. Reaction scheme resulting from the classical dynamics simulations showing the loss of neutral $C_2H_4O_2$ from the C6 site (leading to *m*/*z* 119).

m/*z* 119. Deprotonation of the anomeric centre also results in loss of larger carbon containing neutral fragments. Fig. 7 shows the detailed fragmentation pathways for the fragment anion *m*/*z* 119. Here, deprotonation at OH2 leads to anomeric bond cleavage followed by a proton transfer from the OH5 group to the ring oxygen. This in turn induces the elimination of the neutral fragment HOC_2H_3O through a C4–C5 bond rupture. This agrees with the experiments where 2/3 of the anion PSD signal was shifted to higher masses for 1-^{13}C-D-fructose and 2-^{13}C-D-fructose, and only 1/3 was shifted for 6-^{13}C-D-fructose.

m/*z* 101. The most intense ion observed in ISD appears at *m*/*z* 101. According to our classical dynamics simulations only deprotonation at OH5 results in a fragment ion at *m*/*z* 101. Here the initial deprotonation of OH5 results in antiperiplanar dissociation involving ring-opening between C5 and C4 and cleavage of the C3–OH bond under formation of OH^- (Fig. 8). In a second step, proton transfer from OH4 to the departing OH^- group leads to H_2O formation and further fragmentation into $C_4H_5O_3^-$ (*m*/*z* 101) through anomeric bond cleavage. This corresponds to an exclusive C6 loss, agreeing well with the experimentally observed selectivity. In previous measurements on metastable decay of deprotonated D-fructose and D-ribose [12] it was shown that some fragments appear shifted by one mass unit when comparing ISD and PSD mass spectra. Thus, it is likely that the (metastable) fragment anion at *m*/*z* 101 looses another hydrogen atom after intramolecular redistribution of the internal energy during the flight time to the reflectron to form the ion at *m*/*z* 100. Here it should also be noted that the classical dynamics simulations only cover a time range of 500 fs, i.e. further fragmentation into thermodynamically more favourable products might have been observed if the simulation had run long enough.

m/*z* 89. The signal at *m*/*z* 89 ($C_3H_5O_3^-$) is the most prominent carbon loss channel observed in PSD of the deprotonated D-fructose, and it is also observed with appreciable intensity in the ISD spectra. In the PSD spectra of 1-^{13}C-, 2-^{13}C-, and 6-^{13}C-D-fructose the intensity ratios between *m*/*z* 89 and 90 are all close to 1:1 and no particular selectivity was observed. The simulations showed formation of this ion from the α- and β-D-fructose deprotonated at OH2 and from the α-D-fructose deprotonated at OH1. In the case of deprotonation at OH2 the initial step is an anomeric ring opening followed by a CH_2O loss from C6. A bond rupture between C3 and C4 then leads to a fragment ion at *m*/*z* 89 containing C1, C2 and C3 (Fig. 9a). Deprotonation at OH1 also leads to anomeric ring opening, after proton transfer from OH2. However, then a series

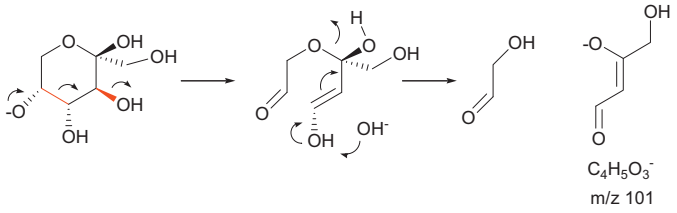

Fig. 8. Reaction scheme showing the formation of $C_4H_5O_3^-$ (*m*/*z* 101) by deprotonation of OH5 as observed in the classical dynamics simulations.

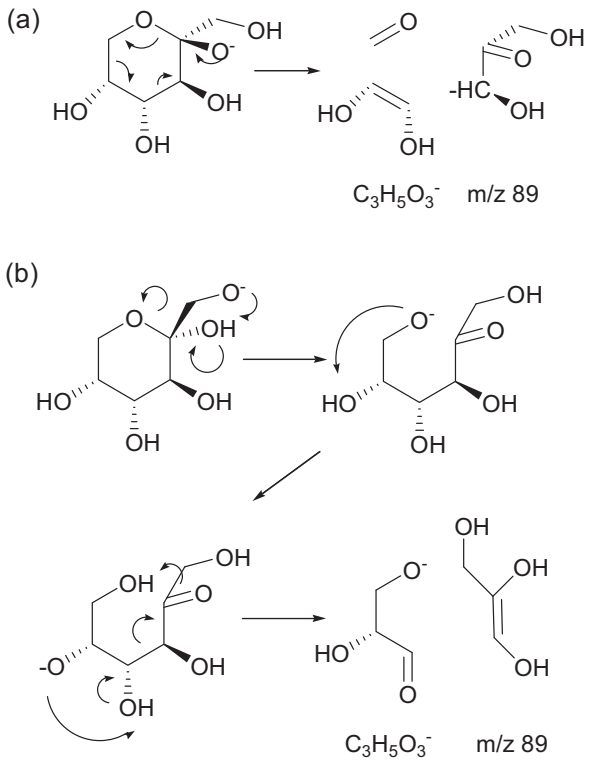

Fig. 9. Reaction scheme from the classical dynamics simulations showing the formation of $C_3H_5O_3^-$ (m/z 89) and $C_4H_7O_4^-$ (m/z 119) by deprotonation of OH2.

of proton transfer reactions leads to C3–C4 bond rupture, and C1, C2 and C3 leave as one unit (Fig. 9b), leaving a m/z 89 fragment containing C4, C5 and C6. This is in very good agreement with our experiment and supports the notation that C1 and C2 leave as one unit.

m/z 59. A fragment ion at m/z 59 was previously observed in MALDI-ISD [12] and dissociative electron attachment [8] experiments on D-ribose, but not from D-fructose. In the current simulations this fragment is observed as the final product after a series of fragmentation steps. Thus, it may be a result of fragmentation with high activation energy barrier, which is not energetically accessible in the experiments, but is seen in the simulations due to the high internal energy (8 eV). To verify this we also carried out simulations where the atomic velocities were scaled to correspond to a total of 5 eV internal energy. These lower energy simulations for β-D-fructopyranose do not show a complex fragmentation resulting in such a small fragment.

4. Conclusions

We studied ISD and PSD of negative ions of D-fructose in MALDI by means of the isotope labelled D-fructose analogues 1-^{13}C-, 2-^{13}C- and 6-^{13}C-D-fructose. By using the isotope labelled D-fructoses we unambiguously identify the composition of most of the fragments observed. To further identify the individual fragments and the fragmentation mechanisms we conducted classical dynamics simulations of the vibrationally excited (hot) α- and β-D-fructopyranose form of D-fructose when deprotonated at the individual hydroxyl groups. We find that ISD proceeds nearly exclusively through terminal carbon loss from the C6 side and the charge remains on the C1 and C2 containing fragment. In PSD other fragmentation channels also contribute and terminal fragmentation from the C1 side competes with carbon loss from the C6 side. The difference in fragmentation pathways is ascribed to the intrinsically different physical character of ISD and PSD. The desorbed ions that are subjected to ISD are considerably hotter and fragmentation proceeds faster than in PSD. The pronounced selectivity in ISD thus is kinetically controlled, whereas the branching ratios in PSD are governed by the thermochemistry.

With our classical dynamics simulations we are able to predict most of the experimentally observed fragmentation products and to elucidate the basic individual dissociation reaction steps behind those. We find that the fragmentation is generally composed of two or all three of the following reaction steps; intramolecular proton transfer, anomeric ring opening and antiperiplanar dissociation. In the simulations we observe that deprotonation at different hydroxyl groups may result in fragment ions with the same m/z ratio but formed via different reaction pathways. This is in accordance with the experimental mass spectra obtained by PSD. There we observe loss of neutral fragments originating from both ends of the molecule, i.e. C1 and C6, for all m/z ratios apart from m/z 101. The simulations suggest that terminal carbon loss from the C1 site contributes when deprotonation occurs at other positions than OH2 (the anomeric centre), namely OH1 and OH5. Deprotonation at the anomeric centre, OH2, on the other hand, predominantly leads to terminal C6 loss. Finally, the simulations show that the fragment ion at m/z 101 (which is the most intense in ISD) originates exclusively from deprotonation at OH5 and there is no alternative reaction pathway to create a fragment ion at m/z 101. In the PSD spectra the only close to 100% site selective reaction channel is observed at m/z 100 and is accordingly assigned to be also due to initial deprotonation at OH5.

Acknowledgements

We acknowledge financial support from the Icelandic Centre for Research (RANNIS), the University of Iceland Research Fund, IB acknowledges support for a visit to Reykjavik by the COST action P9 (Radiation Damage in Biomolecular Systems, RADAM) and by the European Science Foundation (ESF) program: Electron induced processes at the molecular level (EIPAM). HDF acknowledges a PhD grant from the Eimskip University Fund.

Appendix A. Supplementary data

Supplementary data associated with this article can be found, in the online version, at doi:10.1016/j.ijms.2011.05.016.

References

[1] D.J. Harvey, Mass Spectrometry Reviews 18 (1999) 349.
[2] J.P. Simons, R.A. Jockusch, P. Carcabal, I. Hung, R.T. Kroemer, N.A. Macleod, L.C. Snoek, International Reviews in Physical Chemistry 24 (2005) 489.
[3] D.J. Harvey, Mass Spectrometry Reviews 30 (2011) 1.
[4] R.E. March, C.J. Stadey, Rapid Communications in Mass Spectrometry 19 (2005) 805.
[5] K.P. Madhusudanan, Journal of Mass Spectrometry 41 (2006) 1096.
[6] L. Sanche, European Physical Journal D: Atomic Molecular and Optical Physics 35 (2005) 367.
[7] P. Swiderek, Angewandte Chemie (International Edition) 45 (2006) 4056.
[8] I. Bald, J. Kopyra, E. Illenberger, Angewandte Chemie (International Edition) 45 (2006) 4851.
[9] P. Sulzer, S. Ptasinska, F. Zappa, B. Mielewska, A.R. Milosavljevic, P. Scheier, T.D. Mark, I. Bald, S. Gohlke, M.A. Huels, E. Illenberger, Journal of Chemical Physics 125 (2006) 044304.
[10] I. Bald, I. Dabkowska, E. Illenberger, Angewandte Chemie (International Edition) 47 (2008) 8518.
[11] A. Ryzhkova, U. Jarzak, A. Schafer, M. Baumer, P. Swiderek, Carbohydrate Polymers 83 (2011) 608.
[12] I. Bald, H.D. Flosadottir, J. Kopyra, E. Illenberger, O. Ingolfsson, International Journal of Mass Spectrometry 280 (2009) 190.
[13] H. D. Flosadottir, H. Jonson, O. Ingolfsson, in press.
[14] I. Bald, J. Langer, P. Tegeder, O. Ingolfsson, International Journal of Mass Spectrometry 277 (2008) 4.
[15] I. Bald, J. Kopyra, I. Dabkowska, E. Antonsson, E. Illenberger, Journal of Chemical Physics 126 (2007) 074308.

[16] Z.W. Deng, I. Bald, E. Illenberger, M.A. Huels, Angewandte Chemie (International Edition) 47 (2008) 9509.
[17] H.D. Flosadottir, S. Denifl, F. Zappa, N. Wendt, A. Mauracher, A. Bacher, H. Jonsson, T.D. Maerk, P. Scheier, O. Ingolfsson, Angewandte Chemie (International Edition) 46 (2007) 8057.
[18] M. Stano, H.D. Flosadottir, O. Ingolfsson, Rapid communications in mass spectrometry 20 (2006) 3498.
[19] G. Kresse, J. Furthmuller, Physical Review B 54 (1996) 11169.
[20] G. Kresse, J. Hafner, Physical Review B 49 (1994) 14251.
[21] G. Henkelman, A. Arnaldsson, H. Jonsson, Computational Materials Science 36 (2006) 354.
[22] E. Sanville, S.D. Kenny, R. Smith, G. Henkelman, Journal of Computational Chemistry 28 (2007) 899.
[23] W. Tang, E. Sanville, G. Henkelman, Journal of Physics-Condensed Matter (2009) *21*.
[24] J.F. Greisch, V. Gabelica, F. Remacle, E. De Pauw, Rapid Communications in Mass Spectrometry 17 (2003) 1847.
[25] J.A. Kanters, G. Roelofsen, B.P. Alblas, I. Meinders, Acta Crystallographica Section B-Structural Science 33 (1977) 665.
[26] B. Ma, H.F. Schaefer III, N.L. Allinger, Journal of the American Chemical Society 120 (1998) 3411.
[27] L.P. Guler, Y.-Q. Yu, H.I. Kenttaemaa, Journal of Physical Chemistry A 106 (2002) 6754.
[28] J.-Y. Salpin, J. Tortajada, Journal of Mass Spectrometry 39 (2004) 930.
[29] R. Knochenmuss, Analyst (Cambridge United Kingdom) 131 (2006) 966.